HHS Public Access

Author manuscript

Mol Cancer Ther. Author manuscript; available in PMC 2020 August 01.

Published in final edited form as:

Mol Cancer Ther. 2020 February ; 19(2): 564–574. doi:10.1158/1535-7163.MCT-19-0366.

Ceramide-Rubusoside Nanomicelles, a Potential Therapeutic Approach to Target Cancers Carrying p53 Missense Mutations

Sachin K. Khiste[1], **Zhijun Liu**[2], **Kartik R. Roy**[1], **Mohammad B. Uddin**[1], **Salman B. Hosain**[1], **Xin Gu**[3], **Sami Nazzal**[4], **Ronald A. Hill**[1], **Yong-Yu Liu**[1,*]

[1]School of Basic Pharmaceutical and Toxicological Sciences, College of Pharmacy, University of Louisiana at Monroe, Monroe, Louisiana, United States

[2]School of Renewable Natural Resources, Louisiana State University Agricultural Center, Baton Rouge, Louisiana

[3]Department of Pathology, Louisiana State University Health Sciences Center, Shreveport, Louisiana

[4]Department of Pharmaceutical Sciences, Texas Tech University Health Science Center, Dallas, Texas

Abstract

Ceramide (Cer) is an active cellular sphingolipid that can induce apoptosis or proliferation-arrest of cancer cells. Nanoparticle-based delivery offers an effective approach for overcoming bioavailability and biopharmaceutics issues attributable to the pronounced hydrophobicity of Cer. Missense mutations of the protein p53, which have been detected in approximately 42% of cancer cases, not only lose the tumor suppression activity of wild-type p53, but also gain oncogenic functions promoting tumor progression and drug-resistance. Our previous works showed that cellular Cer can eradicate cancer cells that carry a p53 deletion-mutation by modulating alternative pre-mRNA splicing, restoring wild-type p53 protein expression. Here, we report that new Cer-RUB nanomicelles considerably enhance Cer *in-vivo* bioavailability and restore p53-dependent tumor suppression in cancer cells carrying a p53 missense mutation. Natural rubusoside (RUB) encapsulated short-chain C_6-Cer so as to form Cer-RUB nanomicelles (~32 nm in diameter) that substantially enhanced Cer solubility and its levels in tissues and tumors of mice dosed intraperitoneally. Intriguingly, Cer-RUB nanomicelle treatments restored p53-dependent tumor suppression and sensitivity to cisplatin in OVCAR-3 ovarian cancer cells and xenograft tumors

[*]**Corresponding Author:** Yong-Yu Liu, School of Basic Pharmaceutical and Toxicological Sciences, College of Pharmacy, University of Louisiana at Monroe, 1800 Bienville Drive, Monroe, Louisiana 71201, United States, Phone: 318-342-1709, Fax: 318-342-1737, yliu@ulm.edu.

Current address for S.K. Khiste: Department of Medicine, Brigham and Women's Hospital, Harvard Medical School, Cambridge, MA 02139, USA.

Authors' Contributions

Conception and design: Y.Y. Liu, Z. Liu, S.K. Khiste, S. Nazzal, R. Hill

Development of methodology: Z. Liu, Y.Y. Liu, S.K. Khiste,

Analysis and interpretation of data: S.K. Khiste, Y.Y. Liu, K. R. Roy, M.B. Uddin, Z. Liu, S.B. Hosain, X. Gu

Writing, review, and/or revision of the manuscript: Y.Y. Liu, S. K. Khiste, R. Hill, Z. Liu, S. Nazzal

Administrative, technical, or material support: Y.Y. Liu, Z. Liu, S. Nazzal

Disclosure of Potential Conflicts of Interest

No potential conflicts of interest were disclosed by the authors.

carrying p53 R248Q mutation. Moreover, Cer-RUB nanomicelles showed no signs of significant nonspecific toxicity to noncancerous cells or normal tissues, including bone marrow. Further, Cer-RUB nanomicelles restored p53 phosphorylated protein and downstream function to wild-type levels in p53 R172H$^{/+}$ transgenic mice. Altogether, this study, for the first time, indicates that natural Cer-RUB nanomicelles offer a feasible approach for efficaciously and safely targeting cancers carrying p53 missense mutations.

Keywords

ceramide; nanomicelles; p53 tumor suppressor; missense mutation; cancer; drug resistance

Introduction

Ceramide (Cer) is an active sphingolipid metabolite that can function as a tumor-suppressing cellular signal in combatting cancers (1). Cellular Cer, which includes an array of distinct species, is predominantly synthesized by the *de novo* synthesis pathway from serine and palmitoyl-CoA, and is also produced from sphingomyelin breakdown. Cer glycosylation mainly converts Cer into glucosylceramide, catalyzed by glucosylceramide synthase (GCS), and further serial glycosylations generate other glycosphingolipids. In the opposite direction, ceramidase hydrolyzes a Cer to sphingosine, and the latter can further be phosphorylated to sphingosine-1-phosphate (S1P). Increased levels of cellular Cer, attained either by activating Cer synthases in the *de novo* synthesis pathway and sphingomyelinases in sphingomyelin breakdown, or by inhibiting GCS and ceramidases, can result in cell proliferation-arrest, apoptosis and autophagy, thus suppressing tumor growth (1,2). It has been proven that Cer-induced cell death occurs upon treatments with anticancer drugs, or with ionizing radiation, coincidently contributing to therapeutic efficacy (1,2). Inhibition of enzymes involved in Cer metabolism, such as GCS or ceramidases, significantly increases cellular Cer levels, resulting in apoptosis of cancer cells, even drug-resistant ones (3–6). Further, supplying exogenous Cer provides a direct approach for combatting cancers (7–9). Synthetic Cers with short chains are cell-permeable and more efficacious than physiologically prevalent ones with long-chains (i.e., C_{18}-C_{24} Cers) in pushing cells into apoptosis (4,10). It has been reported that Cer-incorporating liposomes could effectively solubilize short-chain Cer, conferring increased bioavailability and anticancer efficacies in tumors (9,11–13). However, natural Cer nanoparticles that not only increase Cer *in-vivo* bioavailability, but also exhibit minimal adverse effects caused by polymeric or other particle constituents, would be highly desirable and have yet to be reported.

Cer cross-talks with tumor suppressor p53 in inducing cancer cell death (14–16). The p53 protein, encoded by the *TP53* gene, functions as a key tumor suppressor that stabilizes the genome with respect to propensity for tumorigenesis and cancer progression. As one essential and powerful transcription factor in cells, p53 activates the expression of p53-responsive genes, including p21, Bax and Puma, and these proteins induce cell death or proliferation-arrest in response to genotoxic stress (17). p53 can upregulate expression of Cer synthase 6 in the *de novo* synthesis pathway, or of neutral sphingomyelinase in the sphingomyelin breakdown route, to directly cause accumulation of cellular Cer (18,19). In

response to genotoxic stress, p53 can also activate the transcription of genes, including members of the Bcl-2 family (Bax, Noxa, Puma), effecting Cer-driven apoptosis of cells carrying wild-type p53 (wt p53) (20). On the other hand, Cer (C_{16}-Cer, for example) can elevate p53 levels, via binding within the p53 DNA-binding domain and disrupting its complex with E3 ligase MDM2, thus decreasing p53 degradation (21). Further, Cer is able to induce apoptosis in WTK1 lymphoblastoid cells that carry p53 M237I mutation by a Cer-dependent pathway, rather than a p53-dependent pathway (22). Our recent studies showed that interventions to increase cellular Cer sensitized cells to anticancer drugs in refractory NCI/ADR-RES (del-21 bp in p53 exon-5) and OVCAR-8 (del-18 bp in p53 exon-5) ovarian cancer cell lines carrying a p53 deletion-mutation (4,14).

It has been reported that the *TP53* gene is mutated in approximately 42% of cases in almost all types of cancers; among these mutations, about 75% are point-mutations that can encode full-length missense proteins (23). *TP53* mutants are often observed in metastatic tumors or in recurred cancers of ovaries and colon (24,25). Point-mutations at codons 175, 248, and 273 constitute approximately 19% of all *TP53* genetic alterations, and these codons are referred to as mutation hotspots, base substitutions at which are more commonly reported in ovaries, colon and lungs (23) (http://p53.free.fr/Database/p53_cancer/all_cancer.html). Missense p53 mutant proteins not only lack the tumor suppression activity of wt p53, but also often exhibit oncogenic gain-of-function (GOF) (17). Transgenic mice having knocked-in *TP53* R172H or R270H mutations (corresponding to R175H or R273H in the human versions) present a broader tumor spectrum with metastases, with compared with mice carrying wt *TP53* (26,27). Li-Fraumeni syndrome (LFS) patients with *TP53* missense mutation develop cancer earlier, and have more tumors and shorter tumor-free survival, than LFS patients without p53(28). Further, recent studies indicated that a heat shock protein 90 inhibitor (17AAG) could suppress mutant p53 levels, and in turn, tumor growth, in colons of mice carrying *TP53* $R248Q^{/+}$ (29,30).

Rubusoside (RUB), a natural steviol glycoside, has successfully served to solubilize various hydrophobic compounds. RUB enabled dispersions of several lipophilic compounds, including paclitaxel and curcumin for *in vivo* studies (31,32). We report herein that we have generated RUB-Cer nanomicelles for delivering C_6-Cer, and assessed bioavailability and effects on xenograft tumors generated from cells carrying a p53 missense mutation.

Materials and Methods

Cer-RUB preparation and characterization

The nanomicelles were prepared via a solvent evaporation method, as described previously (32,33). Briefly, C_6-Cer (or NBD C_6-Cer) and RUB (2:100 ratios in weight) were added and mixed in ethanol (at 1000-fold w/v dilution) for optimal solubility. After filtration, the resulting ethanoic solution was allowed to stand at room temperature (~22°C) for 30 min, followed by evaporation under reduced pressure at 50 °C with agitation in a RAPIDVAP evaporation system until dry powder was obtained (Labconco, Kansas City, MO). This Cer-RUB complex powder was stored at −20 ºC until needed.

For use, Cer-RUB powder was redissolved in deionized water (5 mg/ml), and was further diluted for *in vitro* and *in vivo* studies. *N*-Hexanoyl-*D*-erythro-sphingosine (C_6-Cer) and *N*-[6-[(7-nitro-2,1,3-benzoxadiazol-4-yl)amino]hexanoyl]-*D*-erythro-sphingosine (NBD C_6-Cer) were purchased from Avanti Polar Lipids (Alabaster, AL). RUB was prepared and characterized as described previously (32).

The morphology of the Cer-RUB complex was characterized by transmission electron microscopy (TEM), as described previously (32,33). Briefly, an aliquot of Cer-RUB (10%, w/v) was placed on a 400-mesh carbon-coated copper grid and visualized on a JEOL 100-CX TEM instrument (JEOL Inc., Peabody, MA), with an accelerating voltage at 80 kV. Average particle sizes were calculated for each of three samples, and further corroborated by dynamic light scattering (DLS) using a Zetasizer Nano ZS90 (Malvern Panalytical, Malvern, U.K.) (see Supplementary Materials).

Cell culture

Ovarian cancer cell lines A2780 (wt *TP53*) and OVCAR-3 (missense mutation *TP53* R248Q $^{+/+}$) were purchased from American Type Culture Collection (ATCC; Manassas, VA). Cells were cultured in RPMI-1640 medium (Invitrogen) supplemented with 10% of fetal bovine serum (FBS) for A2780 or 20% of FBS with 0.01 mg/ml bovine insulin for OVCAR-3, and 100 units/ml penicillin, 100 μg/ml streptomycin, and 584 mg/liter L-glutamine. Human MCF-12A mammary epithelial cells were purchased from ATCC, and cultured in Dulbecco's Modified Eagle's Medium-F12 (1:1) with 5% horse serum, insulin (5 μg/ml), hydrocortisone (500 ng/ml), human epidermal growth factor (20 ng/ml) and cholera toxin (100 ng/ml). Cells were maintained in an incubator humidified with 95% air and 5% CO_2 at 37ºC. All cell lines were re-authenticated by short tandem repeat profiling within 3 months of the study, as described previously (33). Cell lines after thawing were cultured with antibiotic-antimycotic (#15240062, ThermoFisher) for 2 passages to prevent mycoplasma contamination; and no testing was performed for mycoplasma species. For all lines, cells in passages 4–15 were used in the described experiments.

Lipid Extraction and HPLC analysis of NBD C_6-Cer

Lipid extraction and Cer analysis were performed as described previously (33). Briefly, OVCAR-3 or A2780 cells (1×10^6 cells/100-mm petri dish) were grown in 10% FBS RPMI-1640 medium for 24 h. After harvest, cells (10^6 cells/reaction) were incubated with 1.0 μM of NBD Cer-BSA or 1.0 μM NBD Cer-RUB in 1% BSA RPMI-1640 medium (200 μl) at 37 ºC for indicated periods. Following rinsing and collection, cells suspended in ice-cold acidic methanol (acetic acid: methanol, 1:50, v/v) were transferred into glass vials and mixed with chloroform and water (1:1:1, v/v/v) to extract cellular lipids. After centrifugation, the organic lower phase was collected and evaporated to dryness, and the resulting residue was then stored at −20ºC until further analysis.

For HPLC analysis, the extracted lipids were dissolved in chloroform/methanol/*ortho*-phosphoric acid solvent (80:20:0.1, v/v/v; 200 fluorescence units in 100 μl). Each sample (5 μl) was loaded onto a normal-phase silica column (5 μm ZORBAX Rx-SIL, 4.6 mm × 250 mm) for separation and analysis. The HPLC system (Agilent 1220 Infinity LC Gradient

System VL) was equipped with an Agilent 1260 fluorescence detector (Agilent, Santa Clara, CA). NBD sphingolipids were eluted by linear gradient (0–14 min, 1 ml/min) formed with solvent system A (chloroform/methanol/*ortho*-phosphoric acid) (80:20:0.1, v/v/v) and solvent system B (chloroform/methanol/H_2O/*ortho*-phosphoric acid) (60:34:6:0.1, v/v/v/v). NBD fluorescence was detected at $\lambda_{excitation}$ 470 nm and $\lambda_{emmission}$ 530 nm, respectively. NBD C_6-Cer in samples was quantitated against a standard calibration curve. Each sample was analyzed in triplicate, and reported Cer levels were as normalized against total cellular or tissue proteins.

Cell viability assay

Cell viability was determined by using the CellTiter-Glo luminescent cell viability assay kit (Promega, Madison, WI), as described previously (4,14). Briefly, cells (4000 cells/well; 2500 cells/well for MCF-12A) were grown in 96-well plates overnight and then switched to 5% FBS medium containing respective drugs for 72 h treatments. For combination treatment, cells were cultured in 5% FBS medium containing Cer-BSA or Cer-RUB (1 μM) and cisplatin (CDDP; 0~15 μM) for 72 h. Cell viability was assessed in a Synergy HT microplate reader (BioTek, Winnooski, VT, USA), following incubation with CellTiter-Glo reagent. NBD C_6-ceramide complexed to BSA (NBD Cer-BSA) was purchased from Invitrogen and cisplatin (CDDP) was procured from Sigma-Aldrich (St. Louis, MO).

Western blot analysis

Western blotting was carried out as described previously (14,34). Briefly, cells or tissue homogenates were lysed in NP40 cell lysis buffer (Biosource, Camarillo, CA) to extract total cellular proteins following these treatments. Equal amounts of proteins (50 μg/lane) were resolved by using 4–20% gradient SDS-PAGE (Life Technologies). The nitrocellulose-membrane blots transferred were blocked in 5% fat-free milk in 0.05% Tween-20, 20 mM phosphate-buffered saline, pH 7.4 (PBST), and then incubated with each one of the primary antibodies (1:500 or 1:5000 dilution), at 4 ºC overnight. These blots were incubated with corresponding horseradish peroxidase–conjugated secondary antibodies (1:5000 dilutions) and detected using SuperSignal West Femto substrate (Thermo Fisher Scientific). Glyceraldehyde-3-phosphate dehydrogenase (GAPDH) was used as a loading control for cellular protein. Antibodies against human p53 phosphorylated at Ser15 were purchased from Cell Signaling Technology (Danvers, MA). Antibodies for Puma, p21Waf1/Cip1, Bax, p53, and GAPDH were obtained from Santa Cruz Biotechnology (Dallas, TX). Relative protein levels were calculated from optical density values for each band, normalized against those for GAPDH.

Animal studies in tumor-bearing mice and transgenic mice

All animal experiments were approved by the Institutional Animal Care and Use Committee, University of Louisiana at Monroe (ULM), and were carried out in strict accordance with good animal practice as defined by NIH guidelines. Athymic nude mice ($Foxn1^{nu}/Foxn1^{+}$, 4–5 weeks, female) were purchased from Harlan (Indianapolis, IN) and maintained in the vivarium at ULM. Animal studies were conducted as described previously (3,4,34). Briefly, cell suspension of A2780 or OVCAR-3 (5–7 passages, 1×10^6 cells in 20 μl/mouse) was subcutaneously injected into the left flank of the mice. Mice with tumors (~2 mm in

diameter) were randomly allotted to different groups (5 mice/group) for treatments. CDDP (1.5 mg/kg, once every 6 days) or Cer-RUB nanomicelles (1 mg/kg, once every 3 days) was administered intraperitoneally (*i.p.*) alone or in combination for 24 days. Mice were monitored by measuring tumor sizes, body weights, and clinical observations, twice a week. Tumor volume was approximated by the formula, $L/2 \times W^2$ (where L is the length and W is the width). Bone marrow cells were extracted from the femurs of mice and counted on a hemocytometer, as described previously (35). Bone marrow cell counts for each mouse were normalized against the body weight.

Heterozygous 129S4-*Trp53*$^{tm2.1Tyj}$ transgenic mice (HTZ, p53 R172H$^{/+}$) that have oncogenesis potential (26,36) and corresponding wt mice (WT) were generously provided by the NCI Mouse Repository (Rockville, MD). Mouse genotypes were identified by amplification of tail DNA using the Platinum™ Blue PCR SuperMix (Invitrogen, Carlsbad, CA) with primers (5' AGC CTG CCT AGC TTC CTC AGG 3'; 5' CTT GGA GAC ATA GCC ACA CTG 3' synthesized by Invitrogen; denaturation, 94 ºC, 1 min; annealing 60 ºC, 2 min; extension 72 ºC, 2 min for 30 cycles), as previously described (26). Cer-RUB nanomicelles (1 mg/kg, *i.p.*, twice in 6 days) or saline were administered to WT and HTZ mice (5 cases/group). Tumors and other tissues were examined and characterized following H&E staining of tissue microsections (5 μm).

Pharmacokinetics experiments

Pharmacokinetics assessments were conducted in mice bearing tumors (A2780 or OVCAR-3; ~5 mm in diameter) generated as described above and previously (9,37). NBD Cer-RUB nanomicelles (1 mg/kg) or NBD Cer-BSA complex (1 mg/kg in medium) was *i.p.*-injected into mice. Blood, tumor and other organs were collected at chosen time-points. Lipids were extracted and analyzed as described above. The pharmacokinetic parameters for noncompartmental analysis were calculated using software PK Solver 2.0.

Flow cytometry analysis

Flow cytometry analysis was carried out as described previously (34,38). Briefly, the resected tumors (~60 mg) were immediately dispersed in medium with collagenase IV (500 units/mL) at 37 °C for 120 min with shaking. Cell suspensions were incubated with CD24 Alexa-Fluor 488-conjugated antibody (5 μl/10^6 cells; mouse IgG1 2F10, R&D Systems, Minneapolis, MN) and CD133/2 APC-conjugated antibody (5 μl/10^6 cells; mouse IgG2b 293C3, Miltenyi Biotec, San Diego, CA) in 1% BSA PBS at 4 °C for 45 min. Tumor cells were resuspended in 1% BSA PBS (1 ml) following washing, and analyzed using a FACSCalibur instrument (BD Biosciences, San Jose, CA). Samples (10,000 events per each) were counted in triplicate. Tumor cells further were smeared on tissue slides, and images captured (200× magnifications) using an EVOS FL cell imaging system with color CCD camera (Life Technologies, Grand Island, NY). The flow cytometry data were further analyzed by using the FlowJo program (v10; FlowJo, Ashland, OR).

Immunocytochemistry

To observe the NBD Cer accumulation, cells (10,000 cells/chamber) grew in a 4-chamber slide with 5% FBS culture medium containing indicated agents for 24 h, and were then

switched to 1% BSA medium containing NBD Cer-BSA (1 μM) or NBD Cer-RUB and incubated for 30 and 240 min. After washing with ice-cold PBS and methanol fixation, cells were counterstained with DAPI (4',6-diamidino-2-phenylindole) in mounting solution (Vector Laboratories). Cells or tissues were observed and images (200× magnifications) captured using an EVOS FL cell imaging system.

For immunostaining of tissue microsections, antigens were retrieved in steaming sodium citrate buffer (10 mM, 0.05% Tween-20, pH 6.0). After blocking with 5% goat serum in PBST, slides were immunostained with primary antibodies against ceramide (1:500) and p21 (1:500), and then Alexa Fluor 488- or 555-conjugated secondary antibodies. Cell nuclei were counterstained with DAPI in mounting solution. Mouse monoclonal antibody against Cer (MID 15B4) was purchased from Sigma-Aldrich, and p21 antibody from Santa Cruz Biotechnology.

Data analysis

All experiments were repeated 2 or 3 times. Data are expressed as mean ± SD. Two-tailed Student's *t*-tests and ANOVA tests were used to compare the continuous variables in groups, using the Prism v7 program (GraphPad Software, La Jolla, CA). All $p<0.05$ comparisons were regarded as statistically significant.

Results

Nanomicelles of Cer-RUB solubilize sphingolipid C_6-Cer in aqueous solution

To enhance the bioavailability of C_6-Cer (Fig. 1A), we encapsulated this sphingolipid with a natural polyglycoside, RUB, that has been applied in prior instances to enhance solubility and bioavailability of drugs (31,32). Due to its pronounced lipophilicity, C_6-Cer is poorly soluble in aqueous solutions, such as RPMI-1640 medium (0.1 mg/ml); however, Cer-RUB complex is soluble, generating a clear, transparent dispersion in medium at a relatively high concentration of 2 mg/ml (Fig. 1B). Based on saturation concentrations in medium and photometry, the solubility of C_6-Cer was increased by more than 1000-fold (5 *vs.* <0.005 mg/ml). With TEM analysis, we found the average diameter of the Cer-RUB nanomicelles to be 32 nm (Fig. 1C). The mean zeta potential and particle size of the Cer-RUB nanomicelles in PBS (pH 7.4, 37 ºC) was −15 mV and 32 nm, respectively, when measured by DLS. Significant changes in particle size and zeta potential of the nanomicelles were not observed upon storage in PBS for 5 days (Fig. S1A, S1B). These results indicate that the Cer-RUB nanomicelles are sufficiently stable as to enable valid experimentation under physiological conditions.

Cer-RUB nanomicelles substantially enhance Cer uptake and bioavailability in cancer cells and in tumors

To examine the impact of Cer-RUB nanomicelles on bioavailability, we firstly assessed cellular uptake of Cer-RUB nanomicelles by cancer cells, comparing with Cer-BSA. In OVCAR-3 cells that carry a p53 R248Q missense mutation, Cer (green) levels in cytoplasm increased in cells incubated with Cer-RUB nanomicelles (1 μM, 240 min) to an approximately 3-fold greater extent than with Cer-BSA (Fig. 2A, 2B). HPLC analysis

further corroborated that Cer-RUB nanomicelles significantly increased Cer levels in OVCAR-3 and A2780 cells (Fig. 2B–2D). Upon incubation with Cer-BSA complex, cellular Cer levels quickly increased, peaking at 60 min, to approximately 530 and 300 fmol/mg in A2780 and OVCAR-3 cells, respectively, and then decreased to 157 and 184 fmol/mg at 240 min. Interestingly, the Cer-RUB nanomicelles gradually and continuously increased cellular Cer during incubations, attaining levels 5-fold (778 *vs.* 157 fmol/mg, $p<0.001$) and 4-fold (665 *vs.* 184 fmol/mg, $p<0.001$) in A2780 and OVCAR-3 cells, respectively, those attained with Cer-BSA complex, after 240-min incubation (Fig. 2C, 2D). The delayed increases of cellular Cer in cells exposed to Cer-RUB are possibly attributable to a protracted release of Cer from endocytosed nanomicelles. Accumulated cellular Cer (areas under curves, AUC) was enhanced by 34% in A2780 and 73% in OVCAR-3 cells incubated with Cer-RUB nanomicelles, as compared to Cer-BSA complex.

We further assessed Cer bioavailability in mice after *i.p.*-administrations of NBD Cer-RUB, comparing with NBD Cer-BSA. At 3 h after administrations, Cer levels were substantially increased, by approximately 28-fold in tumors, 26-fold in kidney, 83-fold in lung, 95-fold in liver, and 55-fold in serum of mice administered Cer-RUB nanomicelles (1 mg/kg) (Fig. 3A), comparing to Cer-BSA complex. The tissue Cer levels of mice administered Cer-BSA were barely detectable with HPLC assays, for instance in tumors (Fig. 3A, 3B). In contrast, administration of Cer-RUB nanomicelles (1 mg/kg) can clearly provide high levels of Cer in most tissues, including xenograft tumors (Fig. 3A, 3B). Further, we found that Cer-RUB nanomicelles equally delivered Cer to tumors and other tissues of mice either bearing OVCAR-3 tumors or bearing A2780 tumors (Fig.3C), except that the Cer levels in brain were much lower (~0.01 ng/mg) than in other tissues (Fig. 3C). Furthermore, our pharmacokinetic studies showed that tissue Cer concentrations reached maximum (C_{max}) in lungs, serum, tumors and colons of mice about 3 h after administration (Fig. 3D). The elimination half-life of NBD Cer ($t_{1/2}$) following the delivery was approximately 6.8 h, and Cer levels in tumors and in serum remained relatively higher after peaking than in lung and colon (Fig. 3D, Table 1).

Cer-RUB nanomicelles sensitize cancer cells carrying p53 R248Q missense mutation to cisplatin

We further assessed the effects of Cer-RUB nanomicelles on cancer drug resistance. Previous reports showed that OVCAR-3 ovarian cancer cells (p53 $R248Q^{+/+}$) were resistant to CDDP and other anticancer drugs (39,40). In the present study, the mean IC_{50} value for CDDP in OVCAR-3 cells was 4-fold greater (3.8 *vs.* 0.84 μM, $p<0.001$) than for A2780 cells that carry only wt p53 (Figs. 4A, 4B, S2A). OVCAR-3 cells also displayed resistance to either Cer-BSA or Cer-RUB: the IC_{50} values were increased 7-fold (6.2 *vs.* 0.9 μM, $p<0.001$) for Cer-BSA, and 3-fold (3.8 *vs.* 1.1 μM, $p<0.001$) for Cer-RUB, as compared to A2780 cells with respective treatments, respectively (Figs. 4A, 4B, S2A). Furthermore, noncancerous MCF-12A cells (wt p53) displayed relative resistance to insult from treatments with CDDP, Cer-BSA or Cer-RUB alone (Figs. S2A, S2B, 4B). As well, RUB itself did not show any cytotoxic effects on any of these cell lines, even at much higher concentrations (>15 μM, Figs. 4A, S2). Interestingly, though, Cer (1 μM) significantly sensitized OVCAR-3 cells to CDDP, as evidenced by reduced IC_{50} values for CDDP in

combination with Cer-BSA (2.3 *vs.* 3.8 μM, p<0.001) or with Cer-RUB (1.1 *vs.* 3.8 μM, p<0.001), respectively (Fig. 4B). However, combination of CDDP with either Cer-BSA or Cer-RUB did not have any significant effect on the IC_{50} values of CDDP in non-cancerous MCF-12A cells (Fig. S2). These results indicate that the re-sensitizing effect of Cer on OVCAR-3 occurs in conjunction with p53 mutation.

Further, we examined the effects of Cer-RUB on tumor growth in mice bearing xenograft tumors of OVCAR-3 or A2780 cancer cells. OVCAR-3 tumors were resistant to CDDP treatments (1.5 mg/kg), and the mean tumor volume was 60% larger (1650 *vs* 1020 mm^3, p<0.001) than what was seen for A2780 tumors (Fig. 4C, 4D). Cer-RUB alone treatments (1 mg/kg) significantly decreased tumor volumes (1253 *vs.* 1650 mm^3, p<0.001) in mice bearing OVCAR-3 tumors (Fig. 4D), but did not significantly reduce A2780 tumors. Furthermore, Cer-RUB nanomicelles sensitized tumors to CDDP inhibition of growth: the mean tumor volume decreased upon combination treatment, to 48% of that seen with CDDP alone (805 *vs.* 1650 mm^3, p<0.001) after 24 days of treatments (Fig. 4D). Flow cytometry analyses of ovarian cancer stem cells (CSCs) in tumors indicated that the fractional CSC population ($CD24^+/CD133^+$) in OVCAR-3 tumors was 2-fold the fraction (0.86% *vs.* 0.4%, p<0.001) found in A2780 tumors of mice treated with CDDP alone (Fig. 4E, 4F). Cer-RUB combined with CDDP significantly decreased CSC fraction in A2780 tumors of mice, by 5-fold (0.08% *vs.* 0.4%, p<0.001), and in OVCAR-3 tumors, by 12-fold (0.07 *vs.* 0.86%, p<0.001) (Fig. 4E). These effects of combination treatments on CSCs were also correspondingly observed in tumor sections upon immunohistochemical staining (Fig. 4F). During animal studies, we did not observe any severe side-effects, and the body weights of treated mice did not present any significant alteration (Fig. S3). Combination treatments with Cer-RUB and CDDP significantly increased bone marrow cells, by approximately 40% (8.7 *vs.* 6.2×10^4 cells/g, p<0.05) as compared to treatments with CDDP alone, in mice bearing either OVCAR-3 or A2780 tumors (Fig. 4G). This observation is interesting given that CDDP often causes bone marrow suppression (41). Treatment with Cer-RUB alone slightly enhanced bone marrow cell numbers, but without significance, in mice bearing OVCAR-3 tumors (Fig. 4G).

Effects of Cer-RUB nanomicelles on the protein expression of *TP53* and p53-responsive genes

To explore how Cer-RUB nanomicelles sensitize OVCAR-3 cells to anticancer drugs and suppress growth of tumors generated therefrom, we assessed treatment effects on the protein expression of *TP53* and p53-responsive genes. The codon 248 missense mutation is among the most common p53 mutants, appearing in approximately 10% of human cancers (IARC TP53 Database version R17). OVCAR-3 cells carry R248Q missense mutation (Arg→Gln) in exon 7 (39,40,42). The wt p53 protein, which can be phosphorylated at serine 15, is barely detected in OVCAR-3 cells or in xenograft tumors generated therewith in mice, in contrast to the situation with A2780 cells or tumors (Fig. 5A–C). Interestingly, we found that Cer, either in Cer-BSA complex or as Cer-RUB, significantly increased the levels of pp53, by 28- or 40-fold, respectively in OVCAR-3 cells, as compared to vehicle treatment (Fig. 5A, 5B). Concordantly, Cer significantly increased the protein levels of p21 and Bax in OVCAR-3 cells treated with Cer-BSA (2-fold, 3-fold) or Cer-RUB (3-fold, 3-fold).

However, Cer did not show such effects on p53 or p53-responsive gene expression in A2780 cells treated with Cer-BSA or Cer-RUB (Fig. 5A, 5B).

In accord with the enhanced *in-vivo* bioavailability of Cer (Fig. 3A), Cer-RUB treatment significantly increased pp53 levels in OVCAR-3 tumors, in comparison to Cer-BSA treatment (Fig. 5C). Consistent with its tumor-suppressing effects (Fig. 4B), treatments with Cer-RUB alone or combined with CDDP significantly increased the levels of pp53, by 4-fold or 6-fold, respectively, as compared to treatment with CDDP alone, in OVCAR-3 tumors (Fig. 5D).

The effects of Cer-RUB on restoration of p53 were further examined in HTZ transgenic mice that carry p53 $R172H^{/+}$ (corresponding to human R175H; identified by genotyping with PCR, bottom panel in Fig. 5E). In colons of HTZ mice, protein levels of pp53 and p21 were very much lower than in WT mice (Fig. 5E). We found that Cer-RUB treatments (1 mg/kg) significantly increased levels of pp53 and p21 in colons of HTZ mice, by 4-fold and 2-fold, respectively, as compared to saline treatments (Fig. 5E). However, Cer-RUB treatments only modestly increased p21 levels, and did not appreciably affect pp53, in the colons of WT mice. Immunohistochemical staining also corroborated the increased p21 expression (red) upon Cer uptake (green) in the cytoplasm of colon cells of HTZ mice treated with Cer-RUB (Fig. 5F). Altogether, these results indicate that Cer-RUB can effectively restore the protein expression of wt p53 and p53-responsive gene in cancer cells or transgenic mice carrying p53 missense mutations.

Discussion

Cer-RUB nanomicelles, in which natural rubusoside encapsulates Cer, succeeded in overcoming hydrophobicity and substantially increasing Cer bioavailability for *in vivo* applications. We did not detect any significant nonspecific toxicity of RUB in cell culture or animal studies, even at significantly higher concentrations or amounts than with the RUB-encapsulated Cer at the highest doses used. By comparison with particles formed with synthetic polymers that have been used to incorporate Cer (9,37,43), the novel Cer-RUB nanomicelles are smaller (32 nm), even though encapsulation efficiency is relative lower (Cer:RUB, 1:50, w/w), and exhibit high water-solubility (>2 mg/ml). Cer efficacy is directly correlated with bioavailability–more specifically, the intracellular or intra-organ Cer levels obtained upon treatments. Cer-BSA complex, which is widely used in cell culture studies, delivered levels of Cer to cancer cells sufficient to reinstate CDDP lethality thereto (Fig. 2B, 2C, Fig. 4A, 4B); however, Cer-BSA could not appreciably deliver Cer into tissues after administration (Fig. 3A, 3B). By contrast, Cer-RUB not only increased delivery of Cer into cultured cells (>3-fold), but also overcame tissue barriers and provided substantial levels into tissues (Fig. 3A). Pharmacokinetics studies further indicate that Cer-RUB nanomicelles can efficiently deliver Cer into tumors and other tissues for various prospective therapeutic purposes (Fig. 3D, Table 1).

In the present study, Cer-RUB nanomicelles specifically sensitized cancer cells carrying p53 missense mutation to anticancer agents. OVCAR-3 cancer cells homozygously carry p53 R248Q and are resistant to many drugs, including CDDP (39,40,42). Cer-RUB comparably

delivered Cer into OVCAR-3 and A2780 cells, or xenograft tumors generated therefrom (Figs. 2D, 3C); however, this nanomicellular agent proved much more efficacious, upon concomitant treatment with CDDP, in killing OVCAR-3 cells, and inhibiting the growth of the generated tumors (Fig. 4), than was the case with wt p53-carrying A2780 cells or tumors. Upon further assessment, the re-sensitizing effects of Cer-RUB correlate with restored protein expression of wt p53 and of p53-responsive genes (p21, Bax) (Fig. 5A–D). Cer-RUB also restored the expression levels of pp53 and p21 in transgenic mice carrying the p53 R172H$^{/+}$ missense mutation (Fig. 5E).

In addition to many cancer cell lines and tumors that present low levels of Cer and are resistant to chemotherapy, enhanced levels of endogenous Cer species (C_{16}~C_{20} carbon chains) have also been observed in patients afflicted with high-grade ovarian serous carcinoma, and in certain breast cancer patients – circumstances associated with cancer aggressiveness (44,45). In light of a “sphingolipid rheostat”, these apparently conflicting findings can be understood from the standpoint that a balance between pro-apoptotic Cer and pro-survival S1P determines cancer cell fate (46). Cancer tissues can break down endogenous Cer via ceramidases to sphingosine which can then be converted via sphingosine kinase into S1P, elevated levels of which are associated with propensity for drug resistance, aberrant proliferation, angiogenesis and metastasis (1,2). In this regard, Cer chain-length clearly matters: not only can exogenously delivered short-chain Cer increase levels of endogenous Cers (47), but it also displays greater potency in inducing cell death, and is slower to be glycosylated, than are longer-chain Cer species (33,48,49). Cer-RUB, shown to effectively deliver Cer for *in vivo* targeting of cancer cells, may improve treatments of at least some cancers, regardless of altered Cer-glycosylation or of the sphingolipid rheostat; however, testing this proposition firstly demands further preclinical studies.

Emerging evidence documents that Cers are involved in restoring tumor suppression activity in cancer cells carrying p53 mutations. Prior studies showed that Cer modulates pre-mRNA alternative splicing so as to restore p53 protein expression and tumor suppression in ovarian cancer cells carrying a p53 deletion-mutation (4,14). Suppression of Cer glycosylation can restore p53-attributable tumor suppression in conjunction with a decrease of N^6-methyladenosine formation in cancer cells carrying the p53 R273H$^{/+}$ mutation (34,50). Most likely, Cer modulates posttranscriptional processes to re-sensitize OVCAR-3 cells carrying the missense R248Q$^{+/+}$ mutation, though the mechanisms still need to be further detailed. Even so, the present study, for the first time, has demonstrated that natural Cer-RUB nanomicelles can efficaciously deliver Cer *in vivo* so as to restore p53-dependent tumor suppression in cases of p53 missense mutations, while sparing normal tissues. The evident potential of Cer-RUB nanomicelles in cancer treatments clearly warrants further investigation.

Supplementary Material

Refer to Web version on PubMed Central for supplementary material.

Acknowledgements

This work was supported by National Institutes of Health Grants P20 GM103424–11 from the National Institute of General Medical Sciences, and R15CA167476 from the National Cancer Institute (to Yong-Yu Liu). This work was also partially supported by funds from the Board of Regents Louisiana (LEQSF-EPS2012-PFUND-299), the Louisiana Campuses Research Initiative (LaCRI-UL/Liu) and the Mizutani Foundation for Glycoscience (120068) (to Yong-Yu Liu). The authors thank Dr. Zhangwei Hu (Department of Medicine, Brigham and Women's Hospital, Harvard Medical School) for his assistance in the dynamic light scattering analysis.

References

1. Hannun YA, Obeid LM. Principles of bioactive lipid signalling: lessons from sphingolipids. Nat Rev Mol Cell Biol 2008;9(2):139–50. [PubMed: 18216770]
2. Ogretmen B Sphingolipid metabolism in cancer signalling and therapy. Nat Rev Cancer 2018;18(1): 33–50. [PubMed: 29147025]
3. Patwardhan GA, Zhang QJ, Yin D, Gupta V, Bao J, Senkal CE, et al. A new mixed-backbone oligonucleotide against glucosylceramide synthase Sensitizes multidrug-resistant tumors to apoptosis. PLoS One 2009;4(9):e6938. [PubMed: 19742320]
4. Liu YY, Patwardhan GA, Bhinge K, Gupta V, Gu X, Jazwinski SM. Suppression of glucosylceramide synthase restores p53-dependent apoptosis in mutant p53 cancer cells. Cancer Res 2011;71(6):2276–85. [PubMed: 21278235]
5. Baran Y, Bielawski J, Gunduz U, Ogretmen B. Targeting glucosylceramide synthase sensitizes imatinib-resistant chronic myeloid leukemia cells via endogenous ceramide accumulation. J Cancer Res Clin Oncol 2011;137(10):1535–44. [PubMed: 21833718]
6. Cheng JC, Bai A, Beckham TH, Marrison ST, Yount CL, Young K, et al. Radiation-induced acid ceramidase confers prostate cancer resistance and tumor relapse. J Clin Invest 2013;123(10):4344–58. [PubMed: 24091326]
7. Zhao X, Sun B, Zhang J, Zhang R, Zhang Q. Short-chain C6 ceramide sensitizes AT406-induced anti-pancreatic cancer cell activity. Biochem Biophys Res Commun 2016;479(2):166–72. [PubMed: 27562715]
8. Wang M, Xie F, Wen X, Chen H, Zhang H, Liu J, et al. Therapeutic PEG-ceramide nanomicelles synergize with salinomycin to target both liver cancer cells and cancer stem cells. Nanomedicine (Lond) 2017;12(9):1025–42. [PubMed: 28440698]
9. Tran MA, Smith CD, Kester M, Robertson GP. Combining nanoliposomal ceramide with sorafenib synergistically inhibits melanoma and breast cancer cell survival to decrease tumor development. Clin Cancer Res 2008;14(11):3571–81. [PubMed: 18519791]
10. Morad SA, Bridges LC, Almeida Larrea AD, Mayen AL, MacDougall MR, Davis TS, et al. Short-chain ceramides depress integrin cell surface expression and function in colorectal cancer cells. Cancer Lett 2016;376(2):199–204. [PubMed: 27045476]
11. Devalapally H, Duan Z, Seiden MV, Amiji MM. Modulation of drug resistance in ovarian adenocarcinoma by enhancing intracellular ceramide using tamoxifen-loaded biodegradable polymeric nanoparticles. Clin Cancer Res 2008;14(10):3193–203. [PubMed: 18483388]
12. Zou P, Stern ST, Sun D. PLGA/liposome hybrid nanoparticles for short-chain ceramide delivery. Pharm Res 2014;31(3):684–93. [PubMed: 24065591]
13. van Vlerken LE, Duan Z, Seiden MV, Amiji MM. Modulation of intracellular ceramide using polymeric nanoparticles to overcome multidrug resistance in cancer. Cancer Res 2007;67(10): 4843–50. [PubMed: 17510414]
14. Patwardhan GA, Hosain SB, Liu DX, Khiste SK, Zhao Y, Bielawski J, et al. Ceramide modulates pre-mRNA splicing to restore the expression of wild-type tumor suppressor p53 in deletion-mutant cancer cells. Biochim Biophys Acta 2014;1841(11):1571–80. [PubMed: 25195822]
15. Liu YY. Resuscitating wild-type p53 expression by disrupting ceramide glycosylation: a novel approach to target mutant p53 tumors. Cancer Res 2011;71(20):6295–9. [PubMed: 21972148]
16. Dbaibo GS, Pushkareva MY, Rachid RA, Alter N, Smyth MJ, Obeid LM, et al. p53-dependent ceramide response to genotoxic stress. J Clin Invest 1998;102(2):329–39. [PubMed: 9664074]

17. Vousden KH, Prives C. P53 and prognosis: new insights and further complexity. Cell 2005;120(1): 7–10. [PubMed: 15652475]
18. Fekry B, Jeffries KA, Esmaeilniakooshkghazi A, Ogretmen B, Krupenko SA, Krupenko NI. CerS6 Is a Novel Transcriptional Target of p53 Protein Activated by Non-genotoxic Stress. J Biol Chem 2016;291(32):16586–96. [PubMed: 27302066]
19. Sawada M, Nakashima S, Kiyono T, Nakagawa M, Yamada J, Yamakawa H, et al. p53 regulates ceramide formation by neutral sphingomyelinase through reactive oxygen species in human glioma cells. Oncogene 2001;20(11):1368–78. [PubMed: 11313880]
20. Jeffries KA, Krupenko NI. Ceramide Signaling and p53 Pathways. Adv Cancer Res 2018;140:191–215. [PubMed: 30060809]
21. Fekry B, Jeffries KA, Esmaeilniakooshkghazi A, Szulc ZM, Knagge KJ, Kirchner DR, et al. C16-ceramide is a natural regulatory ligand of p53 in cellular stress response. Nat Commun 2018;9(1): 4149. [PubMed: 30297838]
22. Shi YQ, Wuergler FE, Blattmann H, Crompton NE. Distinct apoptotic phenotypes induced by radiation and ceramide in both p53-wild-type and p53-mutated lymphoblastoid cells. Radiat Environ Biophys 2001;40(4):301–8. [PubMed: 11820739]
23. Leroy B, Anderson M, Soussi T. TP53 mutations in human cancer: database reassessment and prospects for the next decade. Hum Mutat 2014;35(6):672–88. [PubMed: 24665023]
24. Iacopetta B, Russo A, Bazan V, Dardanoni G, Gebbia N, Soussi T, et al. Functional categories of TP53 mutation in colorectal cancer: results of an International Collaborative Study. Ann Oncol 2006;17(5):842–7. [PubMed: 16524972]
25. Ali AY, Farrand L, Kim JY, Byun S, Suh JY, Lee HJ, et al. Molecular determinants of ovarian cancer chemoresistance: new insights into an old conundrum. Ann N Y Acad Sci 2012;1271:58–67. [PubMed: 23050965]
26. Olive KP, Tuveson DA, Ruhe ZC, Yin B, Willis NA, Bronson RT, et al. Mutant p53 gain of function in two mouse models of Li-Fraumeni syndrome. Cell 2004;119(6):847–60. [PubMed: 15607980]
27. Lang GA, Iwakuma T, Suh YA, Liu G, Rao VA, Parant JM, et al. Gain of function of a p53 hot spot mutation in a mouse model of Li-Fraumeni syndrome. Cell 2004;119(6):861–72. [PubMed: 15607981]
28. Hanel W, Marchenko N, Xu S, Yu SX, Weng W, Moll U. Two hot spot mutant p53 mouse models display differential gain of function in tumorigenesis. Cell Death Differ 2013;20(7):898–909. [PubMed: 23538418]
29. Schulz-Heddergott R, Stark N, Edmunds SJ, Li J, Conradi LC, Bohnenberger H, et al. Therapeutic Ablation of Gain-of-Function Mutant p53 in Colorectal Cancer Inhibits Stat3-Mediated Tumor Growth and Invasion. Cancer Cell 2018;34(2):298–314 e7. [PubMed: 30107178]
30. Alexandrova EM, Yallowitz AR, Li D, Xu S, Schulz R, Proia DA, et al. Improving survival by exploiting tumour dependence on stabilized mutant p53 for treatment. Nature 2015;523(7560): 352–6. [PubMed: 26009011]
31. Liu Z, Zhang F, Koh GY, Dong X, Hollingsworth J, Zhang J, et al. Cytotoxic and antiangiogenic paclitaxel solubilized and permeation-enhanced by natural product nanoparticles. Anticancer Drugs 2015;26(2):167–79. [PubMed: 25243454]
32. Zhang F, Koh GY, Jeansonne DP, Hollingsworth J, Russo PS, Vicente G, et al. A novel solubility-enhanced curcumin formulation showing stability and maintenance of anticancer activity. J Pharm Sci 2011;100(7):2778–89. [PubMed: 21312196]
33. Khiste SK, Hosain SB, Dong Y, Uddin MB, Roy KR, Hill RA, et al. Incorporation of Fluorescence Ceramide-Based HPLC Assay for Rapidly and Efficiently Assessing Glucosylceramide Synthase In Vivo. Sci Rep 2017;7(1):2976. [PubMed: 28592871]
34. Hosain SB, Khiste SK, Uddin MB, Vorubindi V, Ingram C, Zhang S, et al. Inhibition of glucosylceramide synthase eliminates the oncogenic function of p53 R273H mutant in the epithelial-mesenchymal transition and induced pluripotency of colon cancer cells. Oncotarget 2016;7(37):60575–92. [PubMed: 27517620]

35. Bhinge KN, Gupta V, Hosain SB, Satyanarayanajois SD, Meyer SA, Blaylock B, et al. The opposite effects of doxorubicin on bone marrow stem cells versus breast cancer stem cells depend on glucosylceramide synthase. Int J Biochem Cell Biol 2012;44(11):1770–8. [PubMed: 22728310]
36. Yu X, Vazquez A, Levine AJ, Carpizo DR. Allele-specific p53 mutant reactivation. Cancer Cell 2012;21(5):614–25. [PubMed: 22624712]
37. van Vlerken LE, Duan Z, Little SR, Seiden MV, Amiji MM. Biodistribution and pharmacokinetic analysis of Paclitaxel and ceramide administered in multifunctional polymer-blend nanoparticles in drug resistant breast cancer model. Mol Pharm 2008;5(4):516–26. [PubMed: 18616278]
38. Gupta V, Bhinge KN, Hosain SB, Xiong K, Gu X, Shi R, et al. Ceramide glycosylation by glucosylceramide synthase selectively maintains the properties of breast cancer stem cells. J Biol Chem 2012;287(44):37195–205. [PubMed: 22936806]
39. Meijer A, Kruyt FA, van der Zee AG, Hollema H, Le P, Ten Hoor KA, et al. Nutlin-3 preferentially sensitises wild-type p53-expressing cancer cells to DR5-selective TRAIL over rhTRAIL. Br J Cancer 2013;109(10):2685–95. [PubMed: 24136147]
40. Mujoo K, Zhang L, Klostergaard J, Donato NJ. Emergence of cisplatin-resistant cells from the OVCAR-3 ovarian carcinoma cell line with p53 mutations, altered tumorigenicity, and increased apoptotic sensitivity to p53 gene replacement. Int J Gynecol Cancer 2000;10(2):105–14. [PubMed: 11240661]
41. Bartucci M, Dattilo R, Martinetti D, Todaro M, Zapparelli G, Di Virgilio A, et al. Prevention of chemotherapy-induced anemia and thrombocytopenia by constant administration of stem cell factor. Clin Cancer Res 2011;17(19):6185–91. [PubMed: 21868766]
42. Metzinger DS, Taylor DD, Gercel-Taylor C. Induction of p53 and drug resistance following treatment with cisplatin or paclitaxel in ovarian cancer cell lines. Cancer Lett 2006;236(2):302–8. [PubMed: 15990222]
43. Liu X, Ryland L, Yang J, Liao A, Aliaga C, Watts R, et al. Targeting of survivin by nanoliposomal ceramide induces complete remission in a rat model of NK-LGL leukemia. Blood 2010;116(20): 4192–201. [PubMed: 20671121]
44. Moro K, Kawaguchi T, Tsuchida J, Gabriel E, Qi Q, Yan L, et al. Ceramide species are elevated in human breast cancer and are associated with less aggressiveness. Oncotarget 2018;9(28):19874–90. [PubMed: 29731990]
45. Braicu EI, Darb-Esfahani S, Schmitt WD, Koistinen KM, Heiskanen L, Poho P, et al. High-grade ovarian serous carcinoma patients exhibit profound alterations in lipid metabolism. Oncotarget 2017;8(61):102912–22. [PubMed: 29262533]
46. Mandala SM, Thornton R, Tu Z, Kurtz MB, Nickels J, Broach J, et al. Sphingoid base 1-phosphate phosphatase: a key regulator of sphingolipid metabolism and stress response. Proc Natl Acad Sci U S A 1998;95(1):150–5. [PubMed: 9419344]
47. Choi JM, Chu SJ, Ahn KH, Kim SK, Ji JE, Won JH, et al. C(6)-ceramide enhances phagocytic activity of Kupffer cells through the production of endogenous ceramides. Mol Cells 2011;32(4): 325–31. [PubMed: 21874540]
48. Chapman JV, Gouaze-Andersson V, Messner MC, Flowers M, Karimi R, Kester M, et al. Metabolism of short-chain ceramide by human cancer cells--implications for therapeutic approaches. Biochem Pharmacol 2010;80(3):308–15. [PubMed: 20385104]
49. Sassa T, Suto S, Okayasu Y, Kihara A. A shift in sphingolipid composition from C24 to C16 increases susceptibility to apoptosis in HeLa cells. Biochim Biophys Acta 2012;1821(7):1031–7. [PubMed: 22579584]
50. Uddin MB, Roy KR, Hosain SB, Khiste SK, Hill RA, Jois SD, et al. An N(6)-methyladenosine at the transited codon 273 of p53 pre-mRNA promotes the expression of R273H mutant protein and drug resistance of cancer cells. Biochem Pharmacol 2018;160:134–45. [PubMed: 30578766]

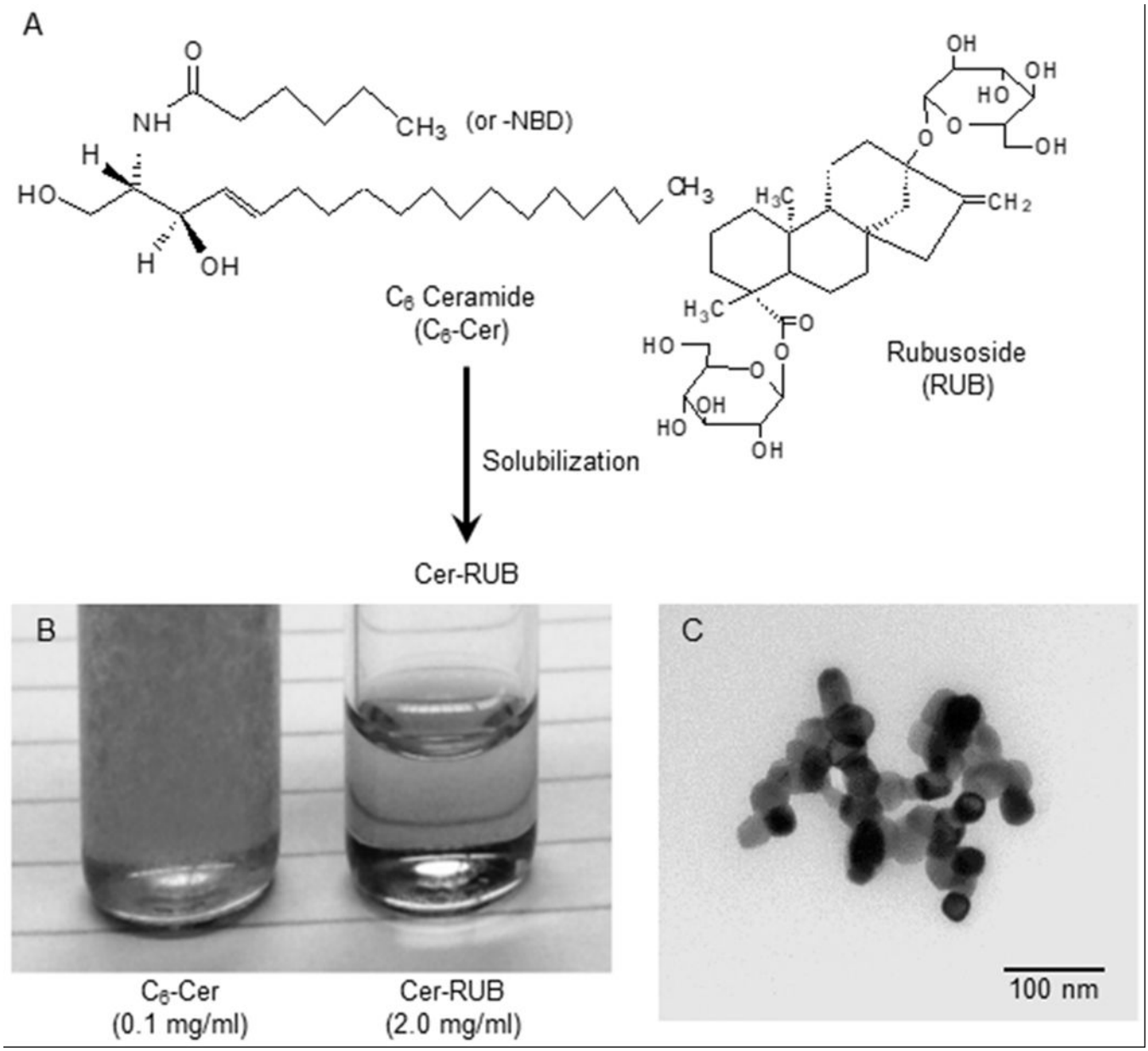

Figure 1.

Characterization of Cer-RUB nanomicelles. **A,** C_6-Cer was encapsulated in RUB, forming Cer-RUB complex (Cer/RUB, 1:20 w/w). **B,** Solubility of Cer-RUB *vs.* Cer. Compared with C_6-Cer (0.1 mg/ml, Left), Cer-RUB (2.0 mg/ml, Right) was dispersed and completely dissolved in RPMI-1640 medium. **C,** Transmission electron microscopy of Cer-RUB nanomicelles (70,000 magnification). TEM images revealed the average diameter of the nanomicelles is 32±4 nm in water.

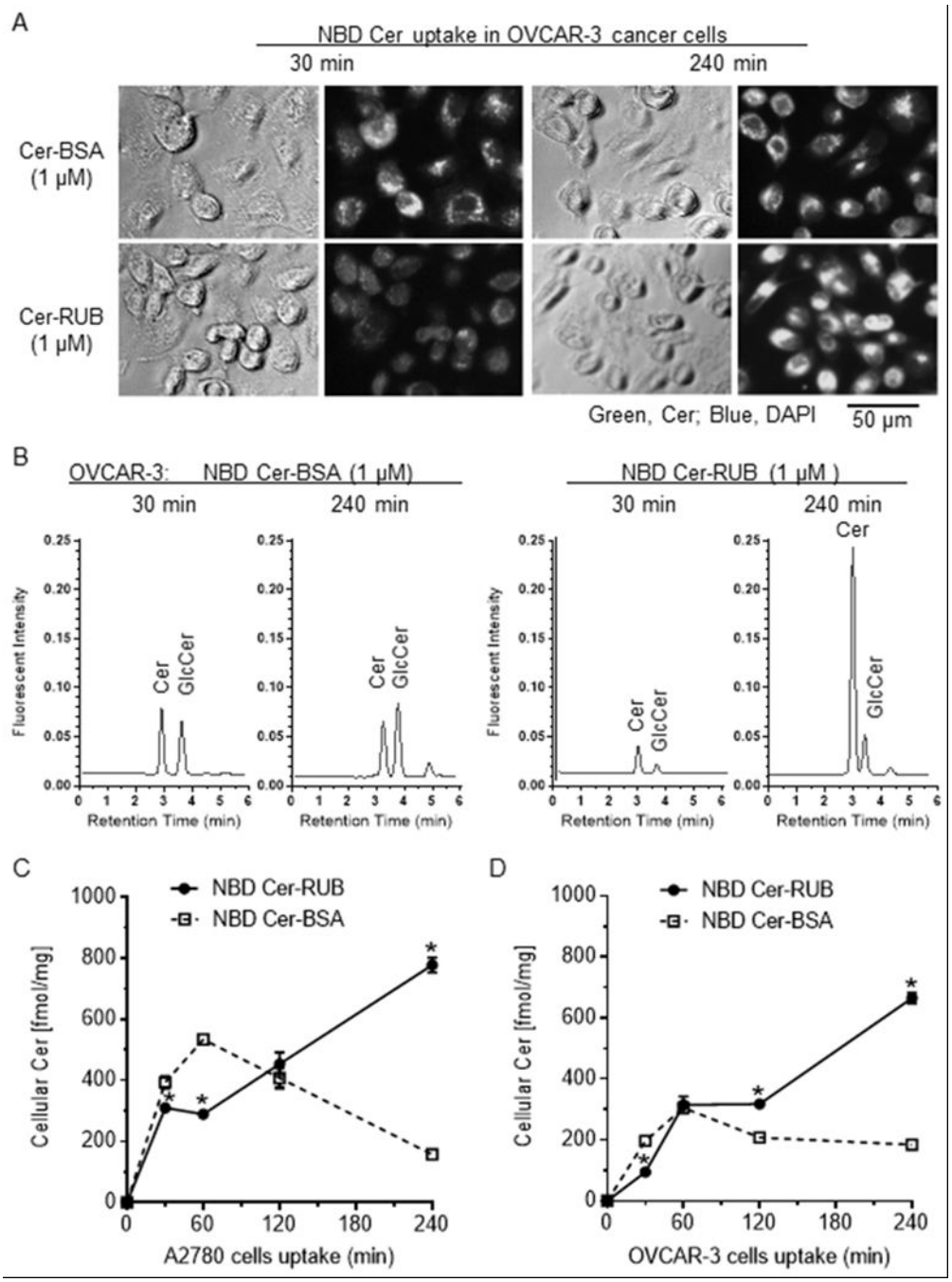

Figure 2.

Uptake of Cer-RUB *vs.* Cer-BSA in ovarian cancer cells. **A,** NBD Cer in cells. After incubations with NBD Cer-BSA complex or NBD Cer-RUB nanomicelles in serum-free medium, OVCAR-3 cancer cells were observed and the photomicrographs (x 200 magnification) were captured by EVOS imaging system. **B,** HPLC chromatograms of cellular NBD C_6-Cer. Lipids were extracted from OVCAR-3 cells incubated with NBD Cer-BSA or NBD Cer-RUB (1 μM; 30, 240 min), and analyzed using HPLC. Cer, NBD C_6-ceramide; GlcCer, NBD C_6-glucosylceramide. **C,** NBD Cer levels in A2780 cells, and **D,** in

OVCAR-3 cells after incubations with NBD Cer-BSA complex or NBD Cer-RUB nanomicelles (1 μM). Cellular Cer levels were assessed using HPLC with NBD C_6-Cer standards. *, $p<0.001$ compared to incubations with NBD Cer BSA complex.

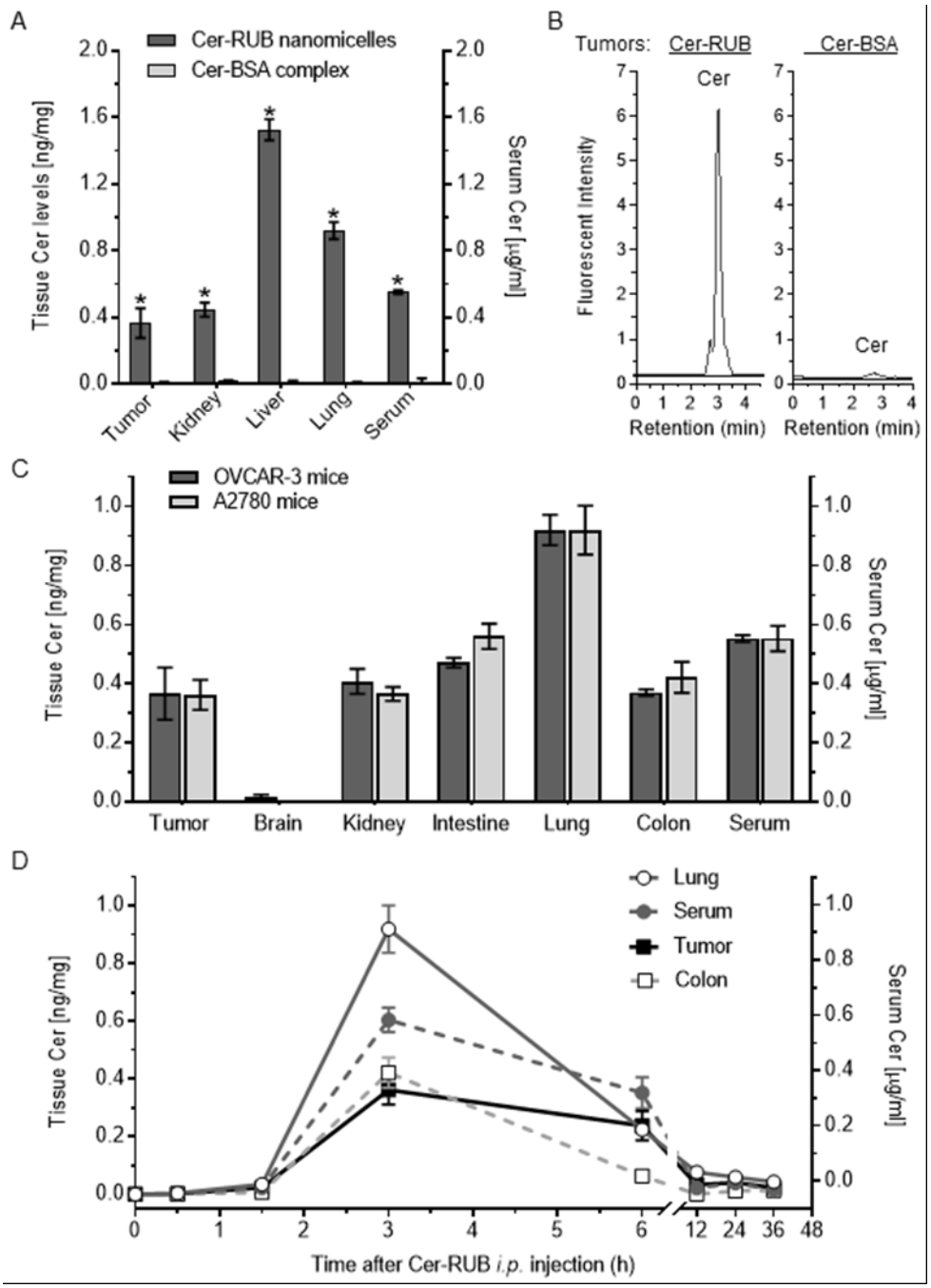

Figure 3.

Cer distribution and pharmacokinetics in mice. NBD Cer-RUB nanomicelles (1 mg/kg in medium; Cer-RUB) or NBD Cer-BSA complex (1 mg/kg in medium; Cer-BSA) were administered *i.p.* into mice (3 cases/group) bearing tumors generated by inoculation with A2780 or OVCAR-3 cancer cells. The lipids extracted from tissues at each time point were analyzed using HPLC. **A,** Cer levels in tissues of mice 3 h after administration. Cer-RUB or Cer-BSA was *i.p.*-administered into mice bearing OVCAR-3 tumors. *, $p<0.001$ compared to mice administered NBD Cer-BSA complex. **B,** HPLC chromatograms of NBD C_6-Cer in

OVCAR-3 tumors of mice 3 h after administrations. **C,** Cer levels in tissues of mice bearing A2780 tumors or OVCAR-3 tumors 3 h following administrations. **D**, Kinetics of C_6-Cer in tissues of mice bearing OVCAR-3 tumors administrated NBD Cer-RUB nanomicelles (1 mg/kg).

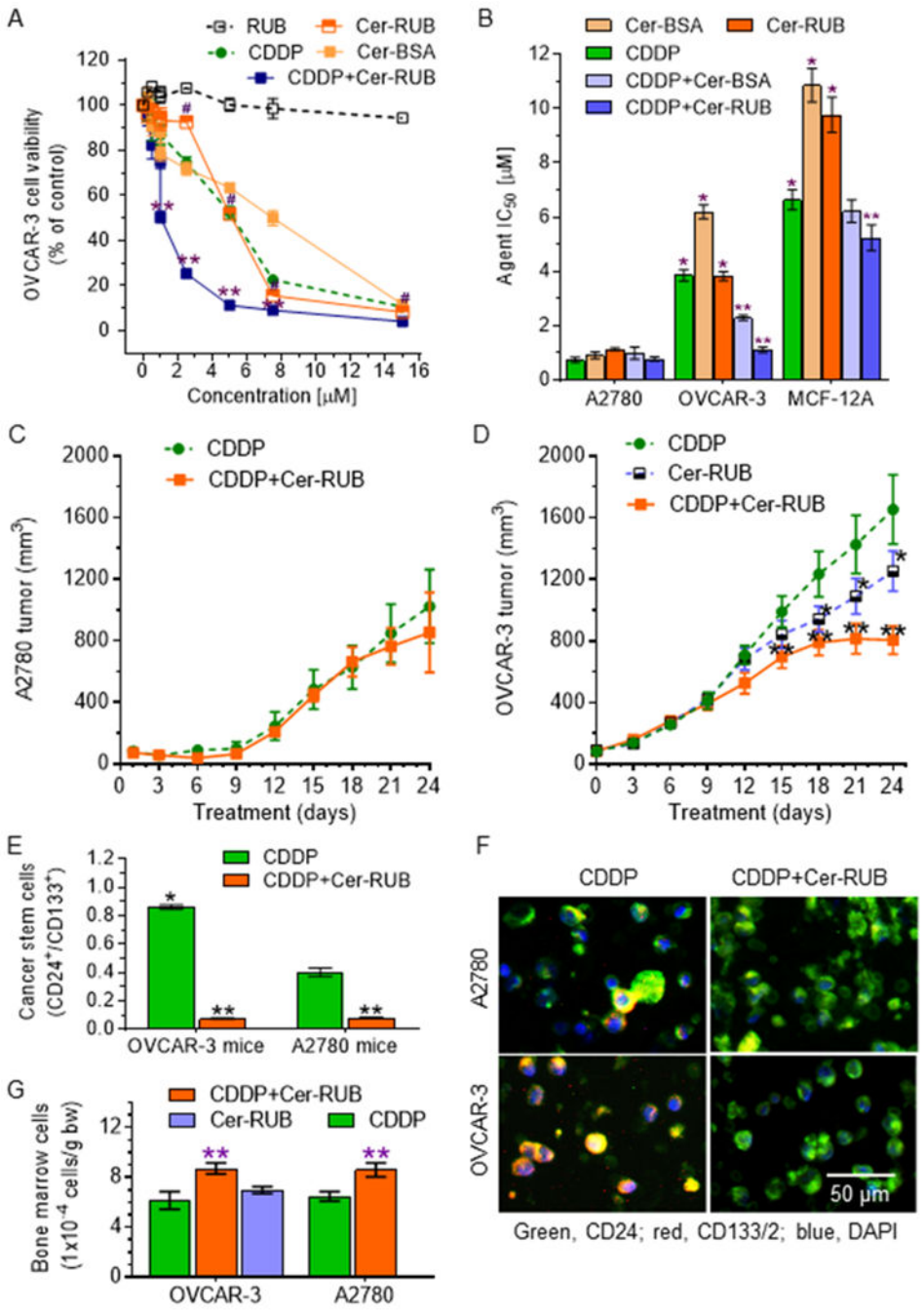

Figure 4.

Effects of Cer on cancer cell response to cisplatin. Cells were treated with Cer-RUB nanomicelles, Cer-BSA complex, RUB alone, or CDDP (alone or combined with 1 μM Cer-RUB or Cer-BSA) for 72 h. **A,** Cell viability of OVCAR-3 cells. #, p<0.001 compared to RUB; **, p<0.001 compared to CDDP or Cer-RUB alone. **B,** IC_{50} values for agents. Cells were treated with each agent alone or CDDP combined with 1 μM Cer-RUB or 1 μM Cer-BSA. *, *p*<0.001 compared to A2780 cells; **, p<0.001 to CDDP alone in OVCAR-3 or MCF-12A cells, respectively. **C,** A2780 tumor growth. **D,** OVCAR-3 tumor growth. Mice

bearing A2780 tumors or OVCAR-3 tumors were treated with CDDP (1 mg/kg, *i.p.* once every 6-days) alone or combined with Cer-RUB nanomicelles (1 mg/kg, *i.p.,* once every 3-days; 5 mice/group). *, $p<0.01$ compared to CDDP treatment; **, $p<0.001$ compared to CDDP or Cer-RUB alone. **E,** Ovarian cancer stem cells in tumors. CSCs were identified as $CD24^{+}/CD133^{+}$ cells by flow cytometry. *, $p<0.01$ compared to A2780 tumors treated with CDDP alone; **, $p<0.001$ compared to OVCAR-3 tumors treated with CDDP alone. **F,** Fluorescence images of ovarian CSCs ($CD24^{+}/CD133^{+}$, yellow) in tumors. Blue, DAPI; green, Alexa Fluor 488-CD24; red, ACP-CD133. **I**, Body weights of mice under treatments. **G**, Bone marrow cells under treatments. bw, body weight; **, $p<0.01$ compared to corresponding mice treated with CDDP or Cer-RUB alone, respectively.

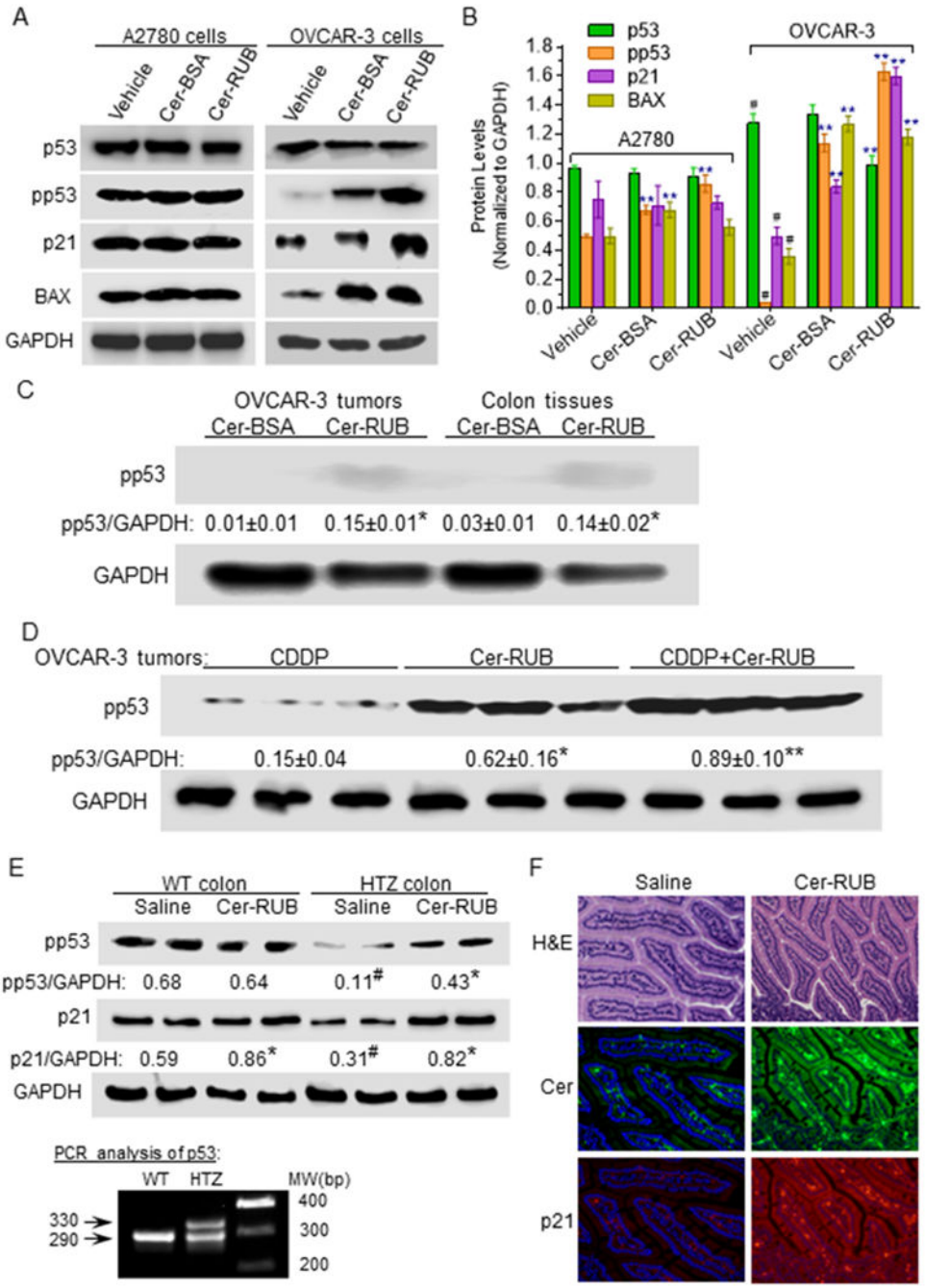

Figure 5.

Effects of Cer-RUB on the protein expression of p53 and p53-responsive genes. **A,** Western blots and **B,** Protein expression levels. A2780 and OVCAR-3 cells were pretreated with Cer-RUB nanomicelles (1 μM), Cer-BSA complex (1 μM) or in vehicle for 4 h, and then co-exposed to CDDP (1 μM) during the last 48 h. Equal amounts of total extracted proteins (50 μg/lane) were used for immunoblotting. #, $p<0.001$ compared to A2780 cells in vehicle; **, $p<0.001$ compared to corresponding cells in vehicle. **C,** Effects of Short-term treatment on phosphorylated p53 (Ser15) levels**.** Mice bearing OVCAR-3 tumors were treated with either

NBD Cer-BSA (1 mg/kg, *i.p.*) or NBD Cer-RUB (1 mg/kg, *i.p.*) for 6 h. *, p<0.001 compared with mice treated with NBD Cer-BSA. **D,** Phosphorylated p53 (Ser15) levels in tumors with prolonged treatments. Mice bearing OVCAR-3 tumors were treated with either CDDP (1 mg/kg, *i.p.* once every 6-days) or Cer-RUB (1 mg/kg, *i.p.,* once every 3-days) alone or in combination for 24 days. *, p<0.001 compared to CDDP; **, p<0.001 compared to Cer-RUB nanomicelles. **E,** pp53 (Ser15) and p21 in colons of transgenic mice. The genotypes of mice used in treatments were verified by extracted tail DNA with PCR. Cer-RUB (1 mg/kg, *i.p.,* twice in 6 days) was administered to wild-type (WT) or HTZ p53 R172H$^{/+}$ transgenic mice. $^{\#}$, p<0.001 compared to WT mice; *, p<0.001 compared to corresponding mice treated with saline. **F,** Immunohistochemistry of colon of p53 R172H$^{/+}$ mice (x 200). Green FL, Cer-Alexa Fluor®488-conjugated antibodies; red FL, p21-Alexa Fluor®555-conjugated antibodies. Nuclei were counterstained with DAPI (blue).

Table 1.

Pharmacokinetics of Cer in mice bearing OVCAR-3 tumors administrated NBD Cer-RUB nanomicelles. t_{max}, time to reach C_{max}; C_{max}, maximum concentration of Cer; $t_{1/2}$, elimination half-life; AUC, area under the concentration-time course.

Tissues	t_{max} (h)	C_{max} (ng/ml or ng/mg)	AUC (ng*h/ml)	$t_{1/2}$ (h)
Serum	3	0.60	3.714	6.82
Tumor	3	0.36	2.83	9.02
Lung	3	0.92	4.77	
Colon	3	0.42	1.63	